Aging due to successive reuse of polyamide 12 powder during laser sintering: extrinsic powder properties and quality of sintered parts

Oluwaseun A. Alo[1], *Iyiola O.* Otunniyi[1] and *David* Mauchline[2]

[1]: Chemical and Metallurgical Engineering Department, Vaal University of Technology, South Africa
[2]: Technology Transfer and Innovation, Vaal University of Technology, South Africa

Abstract. The effects of cumulative build time during the reuse of polyamide 12 (PA 12) for laser sintering (LS) on the morphology, size and shape distribution of the feedstock powder and quality of printed parts were investigated in this study. Both the virgin and reused powders contain potato-shaped, elongated, and relatively few near-spherical particles. In agreement with the scanning electron microscope images, the circularity-roundness plots also indicate presence of near-spherical, potato-shape, and elongated particles in the virgin and reused powders. Particle size distributions of the powders revealed an increase in the proportion of fine particles at higher reuse cycles, which is due to cracking and fragmenting during repeated exposure to the high processing temperature during LS. Mild orange peel was observed at a cumulative build time of 36.4 h, which becomes more evident with increase of the build time. Moreover, the presence of surface defects could be observed at cumulative build times greater than 36.4 h, and all the parts exhibit deviation in average thickness and width from the desired values.

Keywords: Laser sintering, polyamide 12, powder reuse, morphology, shape analysis.

1 Introduction

Laser sintering (LS) is one of the most commonly used additive manufacturing methods. In the LS process, a three-dimensional part is manufactured by using a high-energy laser beam to selectively fuse layers of powdered feedstock material together in a successive manner (figure 1). The process has drawn a lot of attention due to its ability to generate geometrically complex polymeric parts with significantly higher dimensional accuracy and mechanical strength, compared to techniques such as stereolithography and fused filament fabrication [1]. However, the range of polymers suitable for LS is currently limited, with only polyamide 12 (PA 12) taking about 90% of the market share [2]. The cost of PA 12 being more than ten times higher than price of common commodity plastics for injection molding has further limited the wider application of the LS technology [3]. This problem is further complicated

by the low utilization efficiency of PA 12 powder during LS. Moreover, the prolonged exposure of the unused powder to the elevated temperature subjects it to some complex thermo-mechanical stress conditions, which result in alteration of its thermal, rheological, and flow properties that are critical to its further use [4-5]. This makes the direct reuse of the unsintered powder unfavourable and poses a serious material wastage problem, which can lead to both economic losses and environmental pollution. Therefore, despite the growing interests in LS for manufacturing rather than just prototyping, problems associated with poor recyclability and material wastage still need to be addressed to maximize the potential of the process for mass production.

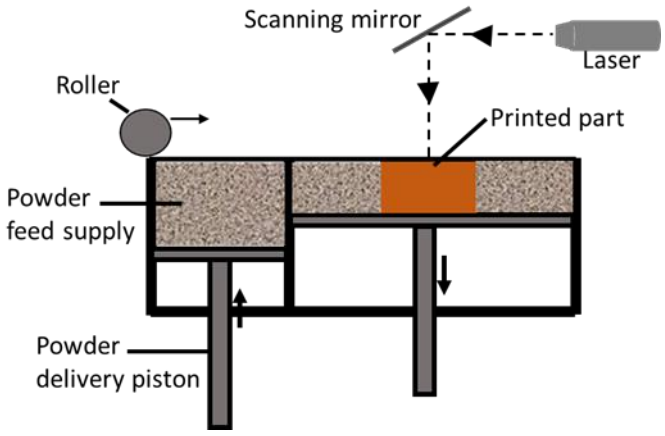

Fig. 1. Schematic representation of laser sintering process [6].

Good powder flowability and spreadability, which are influenced by extrinsic powder properties such as size distribution, shape, and morphology, are critical to achieving quality sintered parts [7-8]. Good powder flowability leads to low particle interactions and smooth powder bed with no surface defect and higher density of the sintered part. In addition, particle size distribution and shape affect the packing density [9]. It has been reported that a bimodal size distribution has a positive effect on the packing density of the layer during LS, since the fine particles occupy the gaps between the coarse particles, which reduces occurrence of big gaps and porosity within the layers [8]. This also leads to increase in the part density and improvement in the mechanical properties of the final sintered part [8, 10]. Intrinsic properties such as melt viscosity and melting and crystallization behavior also play important roles in determining the printability of a polymeric powder and quality of final parts. However, there have been a lot of attention on the extrinsic properties of powders for SLS due to their strong influence on powder flowability and spreadability, and quality of powder bed as well as the geometric and dimensional accuracy, internal stresses, and mechanical properties of laser sintered parts [8, 10-11]. To minimize waste and economic losses in LS of PA 12, an effective and optimal recycling protocol for PA 12 powder is crucial. To achieve this, it is important to determine the extent to which powder properties at each stage of reuse have deviated from those of the virgin powder. Studies have shown that the morphology, size, shape, and surface roughness of PA 12 powder vary with number of reuse cycles due to varying degrees of degradation [12]. Therefore, quantitative information about the variation

of powder characteristics can be obtained by quantitatively monitoring the above properties at each stage of reuse.

There have been reports on effects of reuse on the properties of PA 12 powder and printed parts [12-14]. However, most of these studies only indicated the number of reuse cycles without correlating that with time of exposure to the processing temperature. Other reports [15-17] considered time of exposure of powder but used artificial aging in a temperature-controlled oven, which would result in thermal loads different from conditions in the process chamber in LS machines. This does not only make the reproducibility of the reported state of reused powders (RPs) impossible but limits the practical application of such results. In addition, quantitative description of shape distribution of the powder particles is missing in such investigations. Therefore, despite previous studies on aging and reusability of PA 12 powder during LS, there is still a dearth of information on the quantitative study of how size and shape distributions of the powder varies with the cumulative time of exposure to the processing temperature. In this study, the effects of extent of reuse on the morphology, particle size distribution (PSD), and shape distribution of PA 12 powder during LS and quality of sintered parts were investigated. Extent of powder reuse was expressed in terms of the cumulative build time (t_c), and changes in the powder extrinsic properties at different t_c were correlated with the dimensional accuracy of the printed parts.

2 Aging of PA 12 during LS

The main cause of poor recyclability of used powders during LS is thermal aging**.** Aging of PA 12 during LS is caused by both internal and external factors. The internal factors consist of the thermodynamically unstable state of the polymer, which include incomplete polycondensation or crystallization. The external factors consist of the influence of the environment on the polymer powder, such as energy supply in form of heat or radiation and mechanical stress [18]. Aging of PA 12 powder during LS involves a series of reversible physical and irreversible chemical processes. The physical degradation process is accompanied by change in molecule order, which leads to particle agglomeration, relaxation, and post crystallization. The chemical degradation is predominant and involves phenomena such as chain scission, branching and cross-linking caused by oxidation, post condensation and hydrolysis [4, 19]. Previous studies [20-22] have shown that chemical degradation of PA 12 powders during SLS is mainly due to thermal oxidation (in the presence of oxygen) and post condensation (in the absence of oxygen). The high processing temperature and prolonged exposure time during LS are optimal conditions for chain extension by post-condensation. The high processing temperature in the building chamber promotes increase in chain mobility in the polymer. This offers the possibility for the reactive end groups in the PA 12 to meet and react with each other, which leads to increase in molecular weight [19, 21].

Changes in a polymeric powder during thermal degradation involves phenomena occurring at the molecular and microscopic scales, which then manifest as macroscopic property change. Several authors have focused on the aging behavior of PA 12 during LS and its effects on the powder properties. Drummer et al. [22] investigated the dependency of the rheological behavior of PA 12 powder on time and temperature and found that increase in powder storage time leads to increased viscosity due to post condensation. Chen et al. [5] investigated the degradation mechanism of PA 12 and correlation between deterioration in powder properties and its chemical structure, molecular chain configuration, and crystal structure. The results showed the occurrence of both solid-state and melt-state polycondensation of PA 12 during LS process. Yang and Chen [23] proposed a kinetic model to describe the degradation of PA 12 during LS using a combined theoretical and

experimental approach and considering the effects of both oxygen and laser. The results showed that laser effects are four times stronger than the oxygen effects on PA 12 powder degradation during LS. Chen et al. [24] investigated the processability and recyclability of virgin and aged PA 12 powder in relation to the powder particle size and morphology. The results show that the aged powder exhibit lower particle size and smoother surface compared to the virgin powder. The smoother surface of the aged powder was attributed to premature melting of sharp edge in the particles due to long exposure period and high temperature in the LS building chamber.

3 Methodology

3.1 LS process

The virgin PA 12 (type PA 2200) powder used in this study was supplied by EOS GmbH, Germany. The LS of experimental specimens was carried out using a Formiga P110 (EOS GmbH, Germany) commercial polymer laser sintering system. The laser power (18 W), scanning speed (1500 mm/s), layer thickness (0.1 mm), and build chamber temperature (169 ^{o}C) were kept constant for all the build cycles. For each printing cycle, a constant number of tensile (ASTM D638), flexural (ASTM D790), and dynamic mechanical analysis (DMA) (ASTM D6992) test specimens were printed. After the first build cycle, the unsintered partcake powder around printed parts was removed, sieved, and mixed for homogenization. It was then used for the next build cycle without refreshing with virgin powder.
A total number of 8 build cycles were carried out, after which the build cycle was terminated due to insufficient powder. Samples were collected from the virgin powder and unsintered powder after the second, fourth, sixth, and eighth build cycle for characterization. The cumulative build times were calculated using equation 1:

$$(t_c)_{bn} = t_{b1} + t_{b2} + \ldots\ldots + t_{bi} \qquad (1)$$

Where $(t_c)_{bn}$ is the cumulative build time for nth build cycle and t_{bi} is the build time for ith build cycle. Table 1 shows the value of t_c for the powder samples and printed parts. The value of t_c in Table 1 is the value before the corresponding build cycle. For example, VP represents the virgin powder while RP1 with t_c of 36.4 h represents RP collected after the second build cycle and is used as feedstock for the third build cycle.

Table 1. Cumulative build time and notation for powder samples and printed parts.

Identification of powder	Cumulative build time t_c (h)	Build cycle
VP	0	1st
RP1	36.4	3rd
RP3	56.2	5th
RP5	67.6	7th
RP7	77.0	

3.2 Characterization of Powders and Sintered Parts

As shown in Table 1, five representative samples of the powder and four sintered samples were characterized. The particle size distribution (PSD) of the VP and RP samples from each of the build cycles was determined using a laser diffraction-based Malvern Mastersizer 2000 analyzer. The PSD measurements were repeated three times for each sample and the average results are reported. Scanning electron microscopy (SEM) was carried out on the powder samples. Prior to SEM analysis, the samples were sputter coated with 5 nm of gold to reduce

surface charging in the samples. The SEM images of the powders were used to carry out particle shape analysis using ImageJ software. Figure 2a shows an example of the thresholded image while Figure 2b shows the corresponding image of particles used in shape analysis by imageJ. The shape descriptors evaluated include circularity, aspect ratio (AR), roundness (R), and solidity (S). The surface quality was examined using an optical microscope (Olympus BX 41 with Canon Power Shot G5 camera). To determine the dimensional accuracy, thickness and width of the printed samples were measured using a Craft digital Vernier calliper with an accuracy of 0.01 mm.

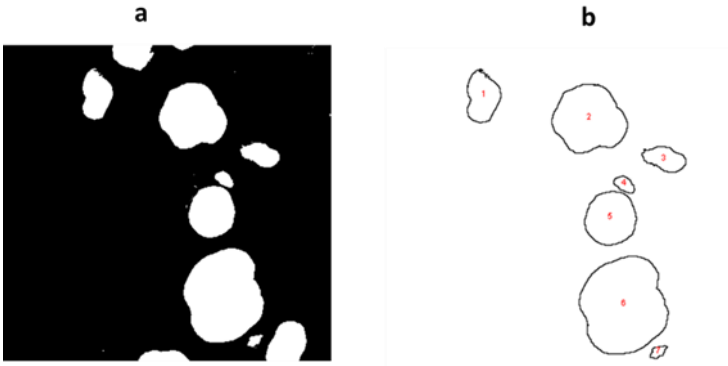

Fig. 2. (a) Sample thresholded binary image; and (b) Image of particles used in shape analysis by imageJ.

4 Results and Discussion

4.1 Morphology of powder particles

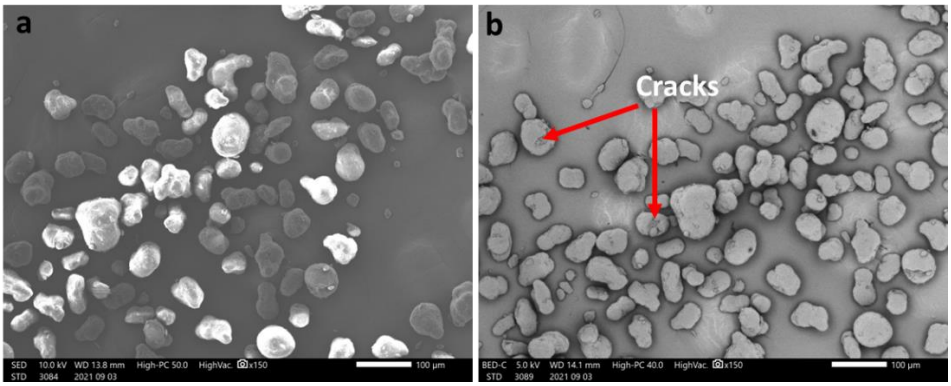

Fig. 3. SEM images showing morphology of virgin powder (a) SE image; and (b) BE image.

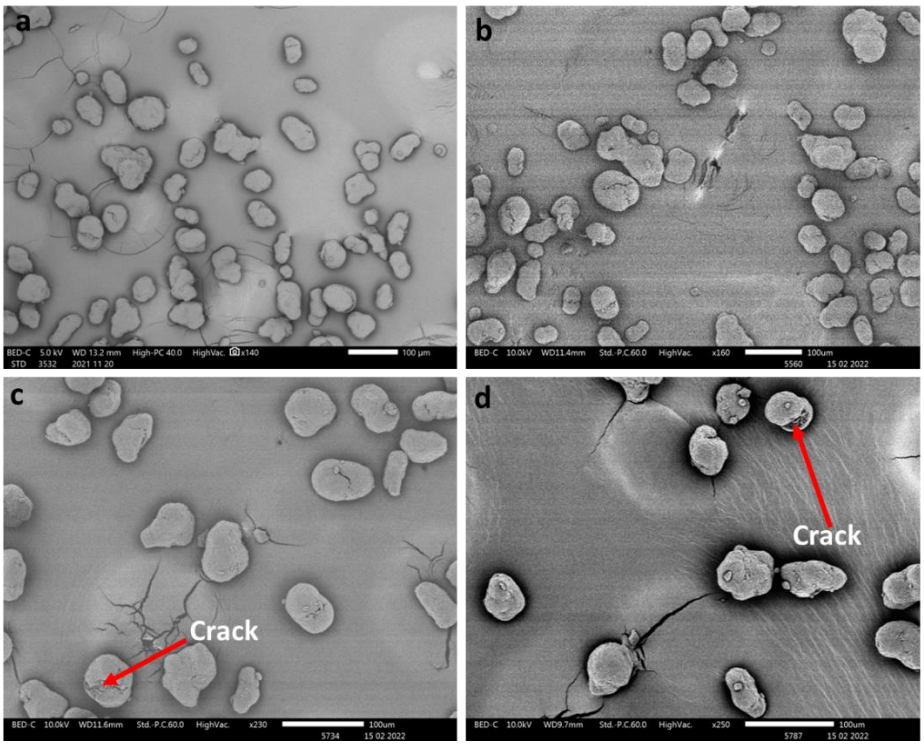

Fig. 4. SEM images showing morphology of reused powders (a) RP1; (b) RP3; (c) RP5; and (d) RP7.

SEM micrographs of the virgin and reused powders (RP1 to RP7) (Figures 3 and 4, respectively) reveal the presence of potato-shaped, elongated, and relatively few near-spherical particles. As shown in the micrographs for the virgin powder, backscattered electron (BE) image (Figure 3a) reveals the surface features of the particles (i.e., presence of cracks and satellite particles) more clearly compared to secondary electron (SE) image (Figure 3b). While cracks in the virgin powder could be attributed to the powder production process, more cracks could be formed in the reused powders due to exposure to repeated LS cycles. Long exposure to high temperature during processing could result in evaporation of absorbed moisture or remaining alcohol from the powder production process, resulting in crack formation.

4.2 Particle Size Analysis

Figure 5a and 5b show the volume-weighted PSD and cumulative volume percent, respectively, of the PA 2200 powders at different t_c (i.e., different extent of reuse). All the powders exhibit a similar size range of 20-150 µm, with slight variations in the volume-weighted PSDs. About 80% of the particles fall in size ranges less than 75 µm. The virgin powder (t_c = 0 h) exhibits a lower proportion of finer particles than the reused powders, with 40.8%, 42.2%, 44.9%, and 43.1% of particles in 50-75 µm size range for powders with t_c values of 0 h, 36.4 h, 61.8 h, and 77 h, respectively. However, proportion of particles in 125-150 µm size range is 0.48%, 0.26%, 0.1%, and 0.13% for the above values to t_c, respectively. Powders with higher proportion of fine particles can be expected to exhibit lower spreadability since small particle sizes lead to greater cohesion between the particles. In addition, the higher cohesive forces associated with smaller particles lead to decreased mobility and flowability [8].

The changes in size distribution due to reuse during LS can be due to partial coalescence under the effect of high temperature and agglomeration due to cohesive forces between particles, leading to an increase in size. On the other hand, mechanical interaction between the powder particles and between the particles and recoater can lead to breaking of particles into smaller particles, especially in particles with severe cracking [8, 24]. The resulting size distribution of a reclaimed powder depends on which of the above two opposing phenomena is predominant. The reclaimed powders are subjected to sieving before each reuse cycle, during which some of the agglomerated and bigger partially sintered particles would be removed. This could lead to the effect of particle fragmenting being more predominant compared to effect of particle coalescence and agglomeration, leading to higher proportion of fine particles in powders with higher reuse cycles. In addition, the repeated cycles of expansion and shrinkage during repeated reuse could lead to powder fragmentation and cracking [25-26]. Higher proportions of finer particles in reused PA 12 powder during LS compared to the virgin powder has also been attributed to particle fragmenting and cracking in previous study [24].

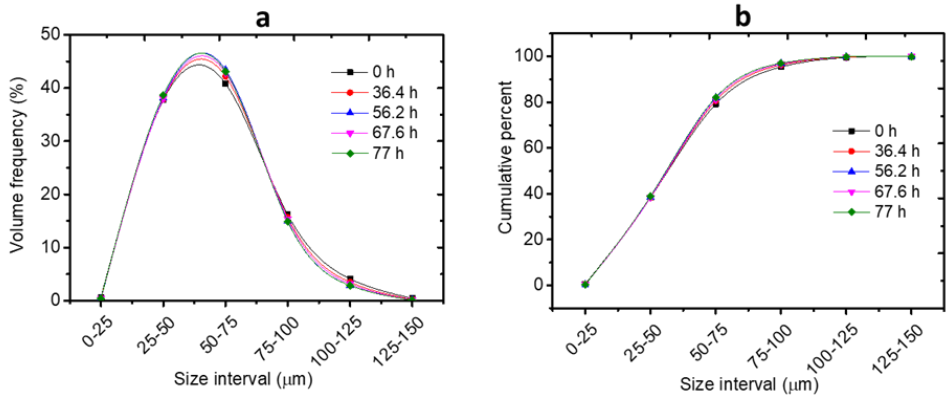

Fig. 5. Variation in PSD of the powders with cumulative build time in terms of: (a) volume-weighted distribution; and (b) cumulative volume percent.

4.3 Particle Shape Distribution of Powders

The particle shape distribution of the powders at varying values of t_c is shown in Figure 6. Circularity distribution of the PA 2200 powders vary significantly with repeated cycles of reuse and increasing time of exposure to the thermal cycles of the LS process (Figure 6a). The virgin powder exhibits the highest percentage of particles in the high circularity range with about 19% of particles with circularity between 0.8 and 1.0. Powders with $t_c \leq 36.4$ h (i.e., VP and RP1) have higher proportions of particles with circularities in the higher range (> 0.5) compared to powder with $t_c \geq 56.2$ h (i.e., RP3 to RP7). Since circularity values close to 1 as much as possible is most favourable for LS, VP and RP1 powders exhibit superior circularity than RP3 to RP7. For all the powders, the proportion of particles with AR in a particular value range decreases and tend to zero as the AR values increases (Figure 6b). Furthermore, increase in number of the reuse cycles and higher t_c leads to higher proportion of particles with AR equal or close to 1 and decrease in the AR distribution width. This could be due to particle breakage and satellite particles segregation, which would lead to higher proportion of low AR-particles and decrease in distribution width with increase in number of reuse cycles.

As shown in Figures 6c and 6d, increase in time of exposure to processing temperature led to change in roundness and solidity distributions of the powders. The reused powders exhibit higher proportions of particles with roundness values in the range 0.6-1.0, compared to the virgin powder. This suggests that the reuse of the PA 2200 yields powders with higher roundness compared to the virgin powder. Particles with near-spherical shape tend to promote good powder flowability and high packing density while powders that consist of particles with irregular shapes exhibit poor flowability and low packing density [11]. The solidity of the powders changed with variation in t_c. Solidity is related to surface roughness of the particle. Particles with very smooth outlines will have solidity close to 1 while those with rough outlines and agglomerated particles tend to have lower solidity values [27]. Therefore, since repeated reuse leads to cracking and fragmenting of LS feedstock powder particles, solidity distribution of the powders would vary as the proportion of particles with cracks and the area of the cracks vary with increasing time of exposure to the thermal cycles of the LS process.

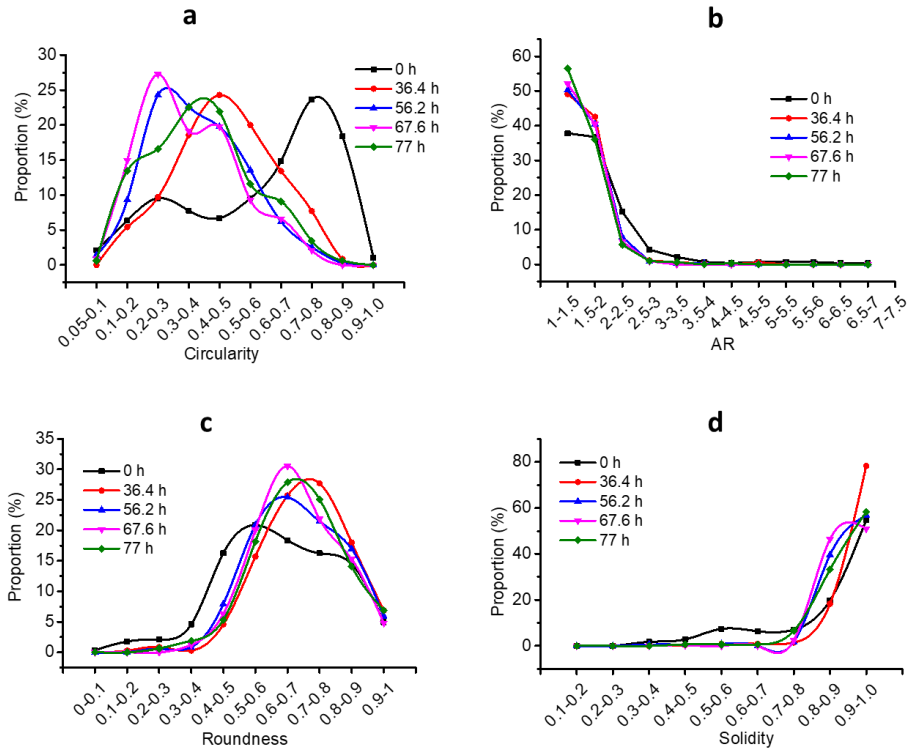

Fig. 6. Variation of distribution of the various shape descriptors with cumulative build time (a) circularity; (b) AR; (c) roundness; and (d) solidity.

Particle agglomeration and fragmentation during LS that lead to change in PSD, would result in particles with different values of the shape descriptors, compared to the parent particle(s). Therefore, the distributions of circularity, AR, roundness, and solidity of the powders would change as the PSD changes with repeated reuse cycles. Since circularity represents the particle's similitude with a sphere while roundness represents the description of the particle's corners, the conformity of the particles with the ideal spherical particle for the LS process can be assessed from the circularity versus roundness plots. As shown in Figure 7, all the powders exhibit no or relatively few particles with high circularity-low roundness (overall circular shape with sharp edges), medium circularity-low roundness

(angular shape with sharp edges), high circularity-medium roundness (sub-rounded overall circular shape), and low circularity-low roundness (elongated shape with sharp edge) combination. Most of the particles in the powders fall within the range of medium circularity-high roundness, medium circularity-medium roundness (sub-rounded and slightly elongated shape), and low circularity-medium roundness (elongated particles with moderately round edges). In addition, relatively few particles fall in the range of low circularity-high roundness (elongated particles with round edges) and high circularity-high roundness, which represents spherical or near-spherical shape, especially in the virgin powder [28].

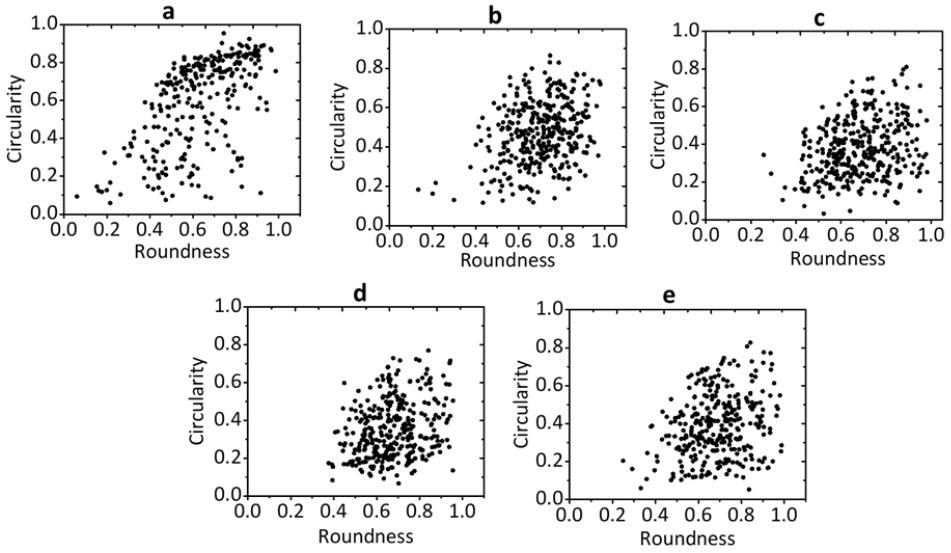

Fig. 7. Plot of circularity against roundness for the virgin and reused powders (a) VP; (b) RP1; (c) RP3; (d) RP5; and (e) RP7.

The particle shape affects the powder flowability and quality of the powder bed. Spherical particles promote good powder flowability and smooth powder bed while irregular and elongated particles lead to poor flowability and coarse surface of powder bed [8, 25]. Therefore, the virgin powder with higher proportion of particles in the spherical or near spherical region of the circularity-roundness plot is expected to exhibit higher flowability compared to the reused powders.

4.4 Quality of Printed Parts

Aesthetic property is a commonly used index for assessing the quality of laser sintered parts. A powder with acceptable level of laser-sinterability must be able to form a part with no or minimal orange peel, which generally manifest in form of substantial surface roughness or pitting [29]. In addition, degradation of powder during LS, which diminishes its subsequent sinterability, generally manifests itself on a directly observable level in the printed part as loss of surface gloss and discoloration [30].

Figures 8a-d show images of the parts printed from the 1st, 3rd, 5th, and 7th build cycles, i.e., parts printed from powders with t_c of 0 h, 36.4 h, 56.2 h, and 67.6 h, respectively. The surface quality of parts diminished as the total time for which the PA 2200 powder has been exposed to the high processing temperature of the LS process (i.e., t_c) increased. A gradual

discoloration, with reference to the part printed from the virgin powder (1st build), could also be observed with increased reuse cycle of powder. A mild orange peel could be observed at t_c of 36.4 h but becomes more evident at higher values of t_c (Figures 8c and 8d). From the optical micrographs in the insets in Figures 8a-d, presence of surface defects (indicated by the arrows) can be seen at $t_c > 36.4$ h (i.e., Figures 8c and d). In addition to part geometry and process parameters, the surface quality of printed parts depends on the roughness and packing density within the powder bed, which are strongly influenced by the feedstock powder characteristics such as PSD and shape distribution [31-32]. For example, insufficient laser energy to fully melt large powder particles may result in partially melted particles, which would lead to surface undulation and roughness in the final sintered part [31-32]. Therefore, the variation in the surface quality of the printed parts can be attributed to the variation in the size and shape distribution with increasing number of reuse cycles. The exposure of the powders to the high processing temperature during LS inevitably causes thermal degradation that decrease their flowability, leading to reduced coalescence and consolidation during printing [20, 33]. This phenomenon become worse as the number of reuse cycle increases, leading to reduced surface quality of printed parts.

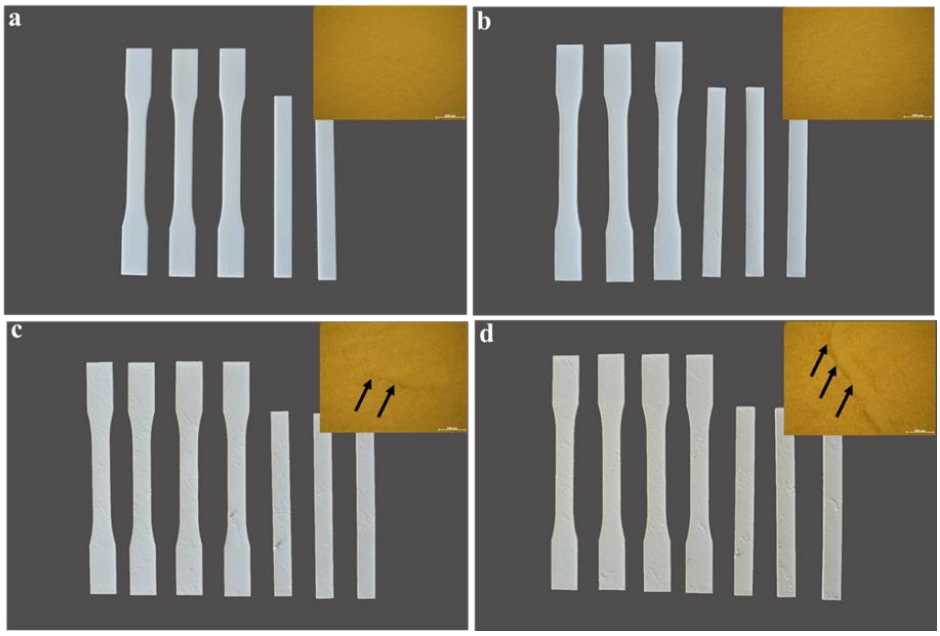

Fig. 8. Variation in surface quality of the printed parts (a) 1st build; (b) 3rd build (c) 5th build; and (d) 7th build. (Insets show corresponding optical micrographs).

Variation in average dimension of the parts was used to assess the effect of repeated powder reuse on the part quality. There is variation in the average thickness and width of the tensile specimen from 3.4 mm at $t_c = 0$ h to 3.6 mm at $t_c = 67.6$ h (Figure 9a) and 12.9 mm at $t_c = 0$ h to 12.7 mm at $t_c = 67.6$ h (Figure 9b), respectively. Similarly, there is variation in the average thickness and width of the flexural specimen from 3.2 mm at $t_c = 0$ h to to 3.4 mm at $t_c = 67.6$ h (Figure 9a) and 12.6 mm at $t_c = 0$ h to 12.7 mm at $t_c = 67.6$ h (Figure 9b), respectively. All the parts exhibit deviation in average thickness and width from the desired values (i.e., thickness of 3.2 mm and 3.0 mm for tensile and flexural samples, and width of 13.0 mm and 12.7 mm for tensile and flexural samples). All the tensile and flexural specimens exhibit higher average thickness than the dimensions in the CAD model, with greater variations in parts printed at higher number of powder reuse cycles. The average width

variation for tensile and flexural samples initially decreased below the nominal dimensions in the CAD models (from t_c = 0 h to t_c = 36.4 h), and then increased. Variation in size and shape distributions of the powders at different stage of reuse would lead to variation in roughness and packing density of the powder bed, and the resulting surface undulations would lead to variation part dimensions [31-32]. The parts sintered from the virgin powder (i.e., t_c = 0 h) exhibit dimensions that are closer to the dimensions of the CAD model compared to parts sintered from the reused powder. This can be attributed to presence of higher proportion of spherical or near spherical particles in the virgin powder compared to the reused powder. However, other factors such as PSD, and surface morphology and chemistry of the particles also influence the final part quality [34].

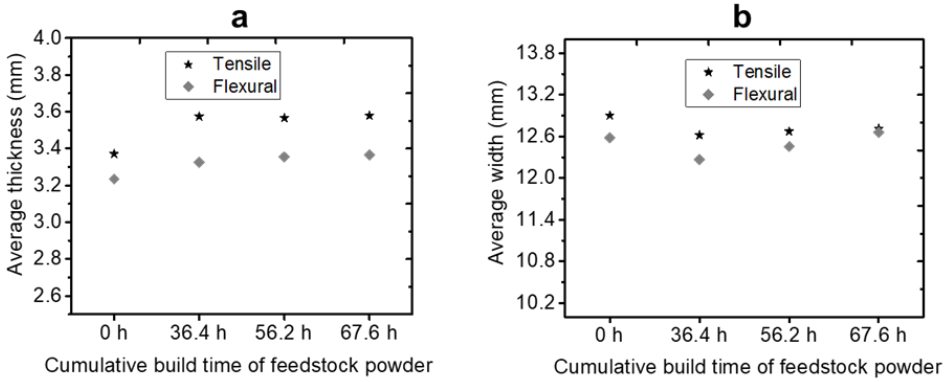

Fig. 9. Dimensional variation of parts printed from virgin and reused powders in terms of (a) average thickness; and (b) average width.

Conclusion

This work investigated the effects of repeated reuse of PA 12 powder during LS on the extrinsic properties of the powder. SEM analysis of both the virgin and reused powders reveal the presence of potato-shaped, elongated, and relatively few near-spherical particles. The virgin powder exhibits a lower proportion of finer particles than the reused powders, which indicates that powder fragmenting during repeated reuse is predominant compared to powder coalescence. The reused powders, on account of their higher proportions of finer particles, can be expected to exhibit inferior flowability and spreadability compared to the virgin powder. There was variation in the distributions of circularity, AR, roundness, and solidity of the powders with repeated reuse cycles since particle agglomeration and fragmentation that lead to PSD change, would also result in particles with different values of shape descriptors, compared to the parent particle(s). Particles with spherical shape exhibit higher flowability and packing density than particles with irregular and elongated shapes. Compared to the reused powders, the virgin powder has higher proportion of particles in the spherical or near spherical region of the circularity-roundness plot and is expected to exhibit higher flowability. Furthermore, the surface quality and dimensional accuracy of the sintered parts decreased with increased number of powder reuse cycles. Mild orange peel could be observed at t_c of 36.4 h but becomes more serious at higher values of t_c. The presence of surface defects could be observed at t_c > 36.4 h. This study provides useful information on the extent to which properties of powders at each stage of reuse have deviated from those of the virgin powder. This knowledge is key to achieving an efficient powder recycling protocol during LS of PA 12.

The work was supported by the Collaborative Programme in Additive Manufacturing (CPAM), South Africa. The authors also acknowledge the support of the Technology Transfer and Innovation and the Department of Chemical and Metallurgical Engineering, Vaal University of Technology, South Africa.

References

[1]. K.V. Wong, A. Hernandez,. ISRN Mech. Eng. 1-10 (2012).
[2]. R.D. Goodridge, C.J. Tuck, R.J.M. Hague, Prog. Mater. Sci. **57**, 2 (2012).
[3]. M. Schmid, K. Wegener, Procedia Eng. **149** (2016).
[4]. A. Wegner, C. Mielicki, T. Grimm, B. Gronhoff, G. Witt, J. Wortberg, Polym. Eng. Sci. **54**, 7 (2014).
[5]. P. Chen, M. Tang, W. Zhu, L. Yang, S. Wen, C. Yan, Z. Ji, H. Nan, Y. Shi, Polym. Test. **67** (2018).
[6]. O.A. Alo, D. Mauchline, I.O. Otunniyi, Adv. Eng. Mater. **24**, 5 (2021).
[7]. M. Van den Eynde, L. Verbelen, P. Van Puyvelde, Powder Technol. **286**, (2015).
[8]. P. Avrampos, G.C. Vosniakos, J. Manuf. Process. **74** (2022).
[9]. S. Ziegelmeier, P. Christou, F. Wöllecke, C. Tuck, R. Goodridge, R. Hague, E. Krampe, E. Wintermantel, J. Mater. Process. Technol. **215** (2015).
[10]. F. Lupone, E. Padovano, F. Casamento, C. Badini, Materials, **15**, 1 (2022).
[11]. Y. Zhou, S. Xi, Y. Huang, M. Kong, Q. Yang, G. Li, Mater. Des. **190** (2020).
[12]. F. Yang, A. Schnuerch, X. Chen, Int. J. Adv. Manuf. Technol. **115**, 9 (2021).
[13]. G. Simha Martynková, A. Slíva, G. Kratošová, K. Čech Barabaszová, S. Študentová, J. Klusák, S. Brožová, T. Dokoupil, S. Holešová, Polymers, **13**, 5 (2021).
[14]. H. Gu, Z. Bashir, L. Yang, Addit. Manuf. **28** (2019).
[15]. K. Dotchev, W. Yusoff, Rapid Prototyp. J. **15** 3 2009.
[16]. A. Martínez, A. Ibáñez, A. Sánchez, M.A. León, *Comparison of aged polyamide powders for selective laser sintering*, in AIP Conference Proceedings, 21-23 September 2011, Cadiz, Spain (2012).
[17]. L. Duddleston, MSc, University of Wisconsin, Madison, 2015.
[18]. J. Benz, C. Bonten, *Temperature induced ageing of PA12 powder during selective laser sintering process, in* AIP Conference Proceedings, 27-29 June 2017, Drensden, Germany (2019).
[19]. K. Wudy, D. Drummer, Addit. Manuf. **25** (2019).
[20]. S. Dadbakhsh, L. Verbelen, O. Verkinderen, D. Strobbe, P. Van Puyvelde, J.P. Kruth, Eur. Polym. J. **92** (2017).
[21]. K. Wudy, D. Drummer, F. Kühnlein, M. Drexler, AIP Conference Proceedings, (2014).
[22]. D. Drummer, K. Wudy, M. Drexler, *Modelling of the aging behavior of polyamide 12 powder during laser melting process, in* AIP Conference Proceedings, 6-12 June 2014, Ohio, USA (2015).
[23]. F. Yang, X. Chen, J. Manuf. Process. **70** (2021).
[24]. P. Chen, H. Wu, W. Zhu, L. Yang, Z. Li, C. Yan, S. Wen, Y. Shi, Polym. Testing, **69**, (2018).
[25]. C. Yan, L. Hao, L. Xu, Y. Shi, Compos. Sci. Technol. **71** (2011).
[26]. S. Yuan, J. Bai, C.K. Chua, J. Wei, K. Zhou, Polymers, **8**, 10 (2016).
[27]. C. Levoguer, *Back to basics: particle characterisation*; Laboratory news (2012).
[28]. S. Berretta, O. Ghita, K.E. Evans, Eur. Polym. J. **59** (2014).
[29]. R. Martinoni, P. Boehler, P. Stenson, Eur. Patent. EP 3536729A1 (2019).
[30]. A.S.D. Shackleford, R.J. Williams, R. Brown, J.R. Wingham, C. Majewski, Addit. Manuf. **46** (2021).
[31]. J.P. Kruth, G. Levy, F. Klocke, T.H.C. Childs, CIRP Annals, **56**, 2 (2007).

[32]. J.P. Kruth, P. Mercelis, J. Van Vaerenbergh, L. Froyen, M. Rombouts, Rapid Prototyp. J. **11**, 1 (2005).
[33]. F. Yang, T. Jiang, G. Lalier, J. Bartolone, X. Chen, Polym. Test. **93** (2021).
[34]. J.S. Weaver, J. Whiting, V. Tondare, C. Beauchamp, M. Peltz, J. Tarr, T.Q. Phan, M.A. Donmez, Addit. Manuf. **39** (2021).